CHALMERS
UNIVERSITY OF TECHNOLOGY

UNIVERSITY OF GOTHENBURG

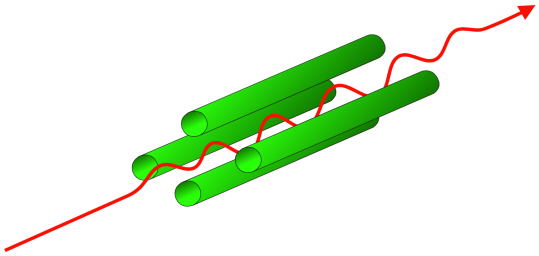

Simulating The Deceleration of Negative Ions in a Quadrupole Beam Guide Using Helium Gas

A thesis presented for the degree of Bachelor of Science

Tarek Alhaskir
Victor Malm
Allan Olesen

Department of Physics

Chalmers University of Technology
University of Gothenburg
Gothenburg, Sweden
June 27, 2021

Simulating The Deceleration of Negative Ions in a Quadrupole Beam Guide Using Helium Gas

A thesis presented for the degree of Bachelor of Science

T. Alhaskir. V. Malm. A. Olesen

Supervisors: Raimund Feifel & Alexander Hinterberger

Project: TIFX04-21-28
Gothenburg
June 27, 2021

GÖTEBORGS
UNIVERSITET

Abstract

Attohallen is a new facility, to be set up by the Department of Physics at the University of Gothenburg, that will be used for exploring the temporal evolution of entangled electrons emitted from atoms and molecules using attosecond chronoscopy and coincidental measurements. An important component of this facility will be a new anion source capable of delivering a high-purity and vibrationally cooled negative ion beam. Simulations of this anion source were performed using SIMION to characterise the behaviour of the components of the ion beamline. A key parameter is the minimum pressure in a quadrupole beam guide that is required pressures, such that the sum of the kinetic and thermal energies of different anion species are reduced to a distribution with full-width half maximum of less than 1 eV, while maintaining a high transmission rate. For masses in a range between 12 and 720 u, a maximal pressure of 10.5 Pa was required. Iterative simulations were used to optimise the electrode voltage to such that anions were effectively guided through the beamline, achieving a total transmission of $\sim$8%. These results have verified the feasibility of the proposed beamline design and yielded valuable insights into the expected gas loads and consequently the required pumping capacity for the planned experiments.

Sammanfattning

Attohallen är en ny facilitet som ska upprättas av institutionen för fysik vid Göteborgs universitet. I denna ska förändringen hos sammanflätade elektroner undersökas under tidsförloppet då dessa emitteras från atomer och molekyler, med hjälp av attosekundkronoskopi och koinsidensanalys. En viktig komponent i denna facilitet kommer att vara den nya anjonkällan, förmögen till att skapa negativa joner kylda till låga vibrationella tillstånd, samtidigt som en hög grad av renhet vidhålls. Simuleringar utfördes i SIMION på denna anjonkälla för att karaktärisera beteendet hos komponenterna i ledet av denna. Huvudsyftet med detta arbete är att bestämma det minimala tryck som krävs i en kvadrupol jonstrålapparatur, för att minska spridningen av summan för kinetisk och termisk energi hos olika anjoner. Fördelningen av energi ska vara så liten som möjligt och inte överstiga 1 eV. För massor mellan 12 och 720 u krävs ett maximalt tryck på 10,5 Pa för att detta ska uppnås. Elektrodspänningsvärden som effektivt leder anjoner genom uppställningen och uppnår en transmission på $\sim$8 % togs även fram. Dessa resultat har lett till värdefull insikt i den förväntade gasbelastningen som krävs i de planerade experimenten, samt verifierat den föreslagna designen.

Acknowledgements

We would like to extend our deepest gratitude for the members of the low density matter physics group at the University of Gothenburg. In special, Raimund Feifel, Alexander Hinterberger, Veronica Ideböhn, Richard Squibb and Sylvain Maclot. Without the support from you, the making of this thesis would not have been possible.

The authors, Gothenburg, June 27, 2021

Contents

Chapter 1

Introduction

1.1 Background

At the beginning of the 20th century, Albert Einstein published his thesis on the photoelectric effect which laid the foundation to analyze atoms and molecules using electron spectroscopy [2]. By these methods it was discovered that atoms and molecules do not behave like any classical particle at all but can instead be described by wave functions, as given by the Schrödinger equation. For systems with one electron this equation works especially well, but for systems with more than one electron we have yet to find exact solutions, for many-body problems are still as unsolvable in quantum mechanics as they are in classical mechanics [3]. These types of problems have to be approached using approximations which require more complex experimental techniques to evaluate. One such method involves using very short-duration light pulses to measure both phase and amplitude of the wave-properties in a system of two or more electrons, in real time. This new method is called attosecond chronoscopy. This time scale is unfathomably small. To put it in perspective, the difference between an attosecond and one second is of the same magnitude as the difference between one second and the age of the universe. These kinds of data together with multi-particle correlation measurements can be used to analyze the temporal evolution of two entangled electrons in real time. The findings could be of great help in understanding precisely the process by which electrons leave an atom or molecule after interacting with electromagnetic radiation. This kind of physical phenomenon occurs in for example plasma, gases and substances in solutions, however, atomic and molecular anions present a particularly attractive and so-far uncharted range of target species, [4].

A new laboratory at the Department of Physics at the University of Gothenburg, Attohallen, will utilize these attosecond pulses to study the electronic properties of negatively charged atoms and molecules. To set up this lab a number of different parts need to be acquired and set up. An important component of this facility will be a new anion source capable of delivering high-purity, vibrationally cooled samples of negative ions. To understand

what requirements each component of this source needs to meet, it is necessary to perform simulations on several parts of the experimental setup.

1.2 Experimental setup

This thesis shall briefly discuss different parts of the full experimental setup, in order to get a better understanding as a whole, before diving into its components.

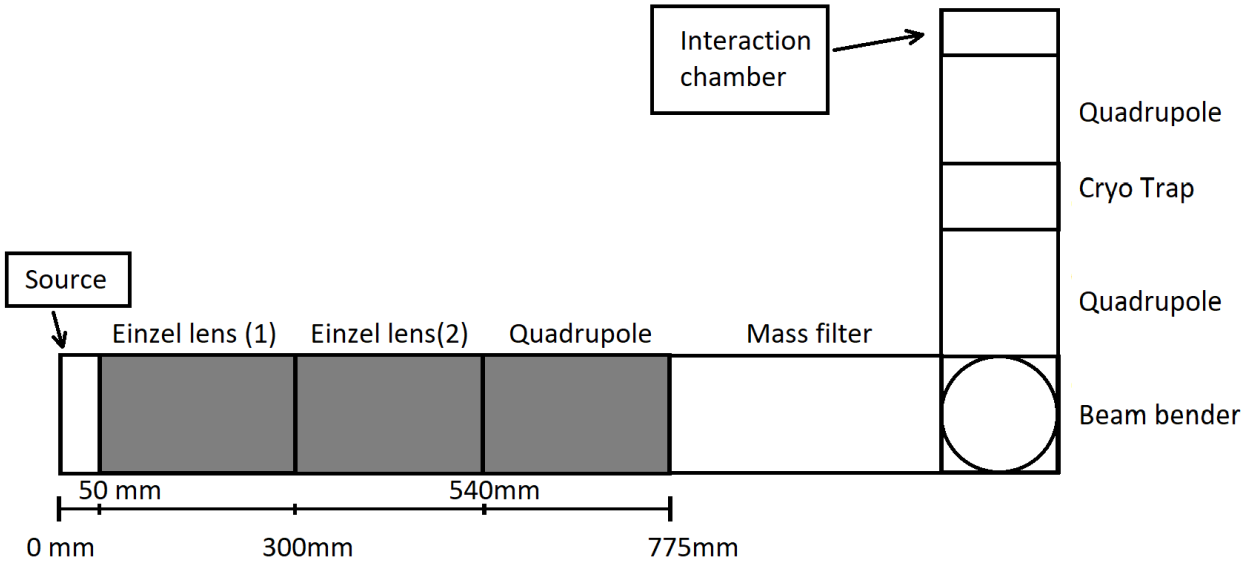

Figure 1.1: Positions of each component in the negative ion setup as well as the scale of the section that this thesis focuses on. This section is marked with gray.

To begin with, a cesium sputtering source (SNICS-II) will be used to create a beam of negative ions. Cesium is first heated in an oven, vaporizing it and coating the entire inside of the source in the process. During this process, the cesium comes into contact with a heated ionizing surface, becoming positively charged. This causes the cesium ions to be launched towards a cathode with a large negative voltage applied in the range of minus 10 kV. A sputtering material is embedded in the cathode which, when bombarded with the cesium cations, produces negative ions that shoot out at a high kinetic energy because of the strong accelerating potential. Different sputtering materials require to be sputtered at different voltages, meaning that the kinetic energy of the beam depends on the target ion species produced [5].

To lower the kinetic energy of the beam, a steep potential gradient is used. After this the beam is focused by Einzel lenses, leading it to a quadrupole beam guide. This beam guide is used to radially stabilize the beam whilst the energy is further decreased to the 1 eV range through collisions with helium gas. Simulations of these steps of the deceleration will be the main focus of this thesis. The workings of this quadrupole is closely related to those of a

Paul trap, first demonstrated in 1962, where it was used to confine and analyze helium ions under the influence of a spin polarized cesium beam [6, p.5].

Because the source does not solely produce one kind of ion, a mass filter is used to homogenize the beam such that it only contain ions of a similar mass. Neutral particles can stem from the source and there is also the possibility that ions can be neutralized during flight. Because of this, a beam bender is used to remove neutral particles.

The remaining ions are still hot and must be cooled down to the desired temperature of 50 K, which leads to the next component: the cryotrap. This component cools the ions by trapping them in the presence of a cold head, fed with chilled helium. This is required to be able to reach temperatures as low as 50 K. The reason to cool the ions to such a low temperature is to keep them in their vibrational and electronic ground state. If the temperature is increased there is a higher possibility of excitation, influencing the ions' electronic structure and properties, thus altering the results.

These components will be sectioned off with walls to have a higher degree of control over the vacuum in each section. Gas is only required in the compartments housing the cryotrap and the first quadrupole but it is inevitable that some will leak through into other sections of the apparatus.

When the ions have been cooled to the desired temperature, they are extracted into the interaction chamber of an electron spectrometer, where negative ions are analyzed using photodetachment and photoionization.

1.3 Purpose and aim

The main goal of this thesis is to computationally determine the pressures required in order to decrease the energy of a beam of negative particles. This data will be vital to estimate the specifications required for the differential pumping such that the pressure in is kept low, except for in the compartments housing the first quadrupole and the cryotrap.

The pressure needs to be calculated for different masses corresponding to different substances that will be analyzed in the new laboratory. The masses 12, 50, 100, 400 and 720 u have been selected by the group as the most important masses to simulate based on the species that are expected to be analyzed in the new facility. After exiting the quadrupole, each beam of ions needs to have a mean kinetic energy of around 1 eV and the energy spread of the particles should not exceed 1 eV.

A couple of parameters are needed to be determined before the data of the pressure required in the quadrupole can be extracted. First, the voltages for the two Einzel lenses used after the source to focus the beam through holes into the next sections must be optimized. When the transmission through to each section has been maximized, the parameters for the quadrupole need to be determined. A potential gradient is applied to make sure the negative particles leave the quadrupole since there is a risk of ions getting stuck in this section. When all of

these parameters have been determined, more rigorous simulations can be done to acquire the desired data.

Chapter 2

Theory

2.1 Charged particle traps

A charged particle trap is useful to contain and control very small and fast moving particles with a net charge. They can be used for capturing charged particles, mass selection or to guide particles down a specific path. A Paul trap is one such trap, that uses only electric fields to trap the particles, in this section the theory behind which will be discussed.

2.1.1 The Paul trap

Paul traps come in many shapes and sizes but a very common design is a trap with hyperbolic electrodes [6, p.14]. It consists of three electrodes: a ring and two hyperboloid shaped end caps as seen in figure 2.1. This is the original design made by Wolfgang Paul and it allows for 3-D confinement of charged particles.

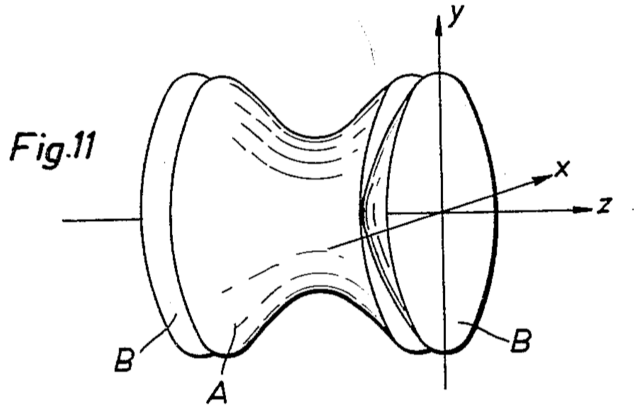

Figure 2.1: Paul trap with hyperbolic electrodes. The geometry allows for three dimensional trapping of ions. A is the ring and B the end caps. Sketch from original patent [7].

Another common design also made by Wolfgang Paul is the quadrupole- or linear Paul trap. In this type of trap, four rods, either circular or hyperbolic in shape, are used together with two end caps in order to achieve 3-D confinement [6, p.109]. Radio-Frequency (RF) voltages, as well as an optional DC voltage, are applied to the electrodes such that the opposite pairs of electrodes have the same voltage, see figure 2.2. The benefit of this design is that more ions can be trapped due to the larger internal volume of the trap. The design can also be modified to only allow two dimensional trapping if the end caps are removed. In this way the trap is transformed into a quadrupole beam guide allowing a beam of charged particles to propagate while still being confined radially.

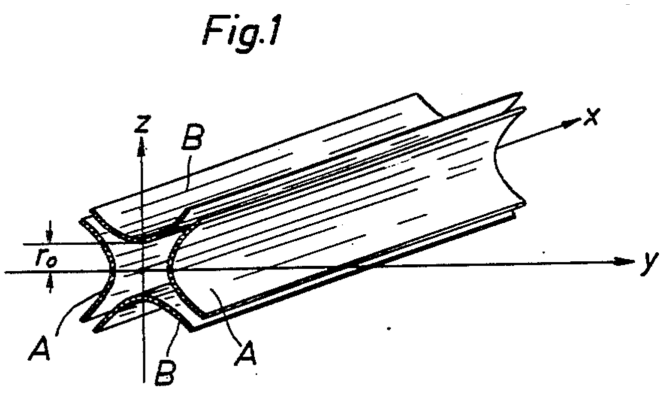

Figure 2.2: Quadrupole beam guide with hyperbolic rods. The A and B rod pairs would have negative and positive voltages applied respectively. r_0 is the distance from the center to the closest point of the rod. Sketch from original patent [7].

The Paul trap works by applying a voltage of the form $U_0 + V_0 \cos(\Omega t)$ between either the ring and end caps or in between the rods [6, p.17]. For each half-cycle of the RF component of the voltage, the electric field is rotated 90 degrees. This in effect creates an electromagnetic version of the mechanical rotating saddle point, which is illustrated in figure 2.3 and 2.4, where the electric field and the resulting potentials acting on the ions are marked. Because of the oscillating field, the force acting on the ions is not necessarily zero over time, instead depends on the position and trajectory of the ions. If the frequency is just right, the fields will create a region of space where the force will always push the ions towards the center.

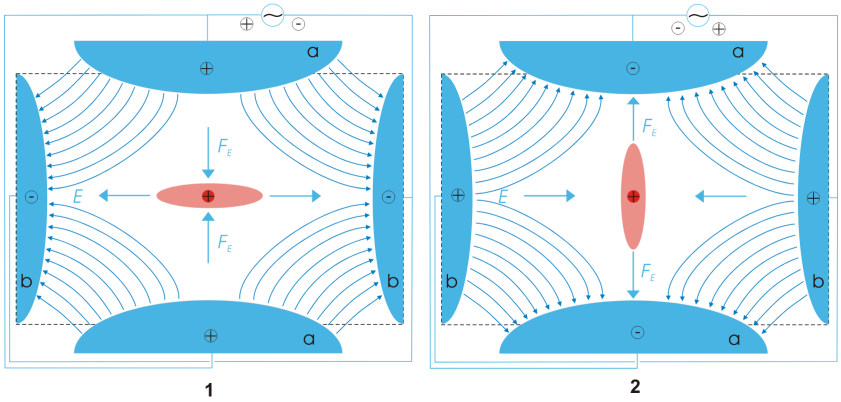

Figure 2.3: Rotating field lines in a quadrupole. Electric field lines and the direction of the resulting force acting on the ions can be seen. The red ovals represents a cloud of ions and in blue are the ring and end caps. Figure 1 represents the field at $t = 0$ and figure 2 at $t = \frac{1}{2}$ T, were t is the time and T is the period of the oscillation [8].

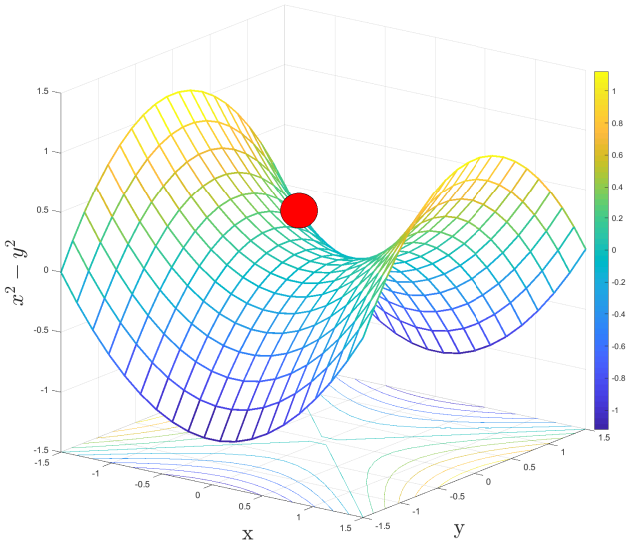

Figure 2.4: Saddle potential created by a Paul trap or quadrupole beam guide. If the potential portrayed were static the ball display would roll down the side, however if the potential were to be inversed (or rotated 90 degrees) the ball would be redirected towards the center again. This type of rotation occurs back and forth consecutively in these types of traps.

2.1.2 Trapping stability

$$a_{\mathrm{x}} = -a_{\mathrm{y}} = \frac{4QU_0}{Mr_0^2\Omega^2}, \qquad q_{\mathrm{x}} = -q_{\mathrm{y}} = \frac{2QV_{\mathrm{rf}}}{M{r_0}^2\Omega^2}, \tag{2.1}$$

In equation (2.1) Q is the charge of the trapped particle, U_0 is the possible diagonal offset voltage (non-zero for mass selection), M is the mass, r_0 is the distance from the center of

the trap to the closest point on the electrodes, Ω is the angular frequency of the RF-drive and V_{rf} is the voltage of the RF-field. These parameters only apply to a linear quadrupole trap, were ions are confined in two dimensions radially.

It is possible to determine the stable regions of a Paul trap. To do so in a linear Paul trap for positions far from the end caps, the static and oscillating fields created by the applied voltages are used, from which the resulting potential can be obtained. Using this potential to obtain the equations of motion for a single ion solely in the x-y-plane, the conditions for stable confinement can be obtained. If the a-q-parameters presented above in equation (2.1), are substituted into the equations of motion it yields a system of differential equations in the form the Mathieu equation for which a general solution exists [1] [6, p.16, 111].

As it turns out, the stability of the solutions of the Mathieu equation depend only on the a-q-parameters [6, p.19]. Dividing the a-q-plane into stable and unstable regions results in the periodic function plotted below in figure 2.5. The overlapping regions show where stable confinement can be obtained. The most important which is the first region of stability, the one closest to the origin, where the ions will be trapped since it is the largest region and therefore offers more control of the parameters.

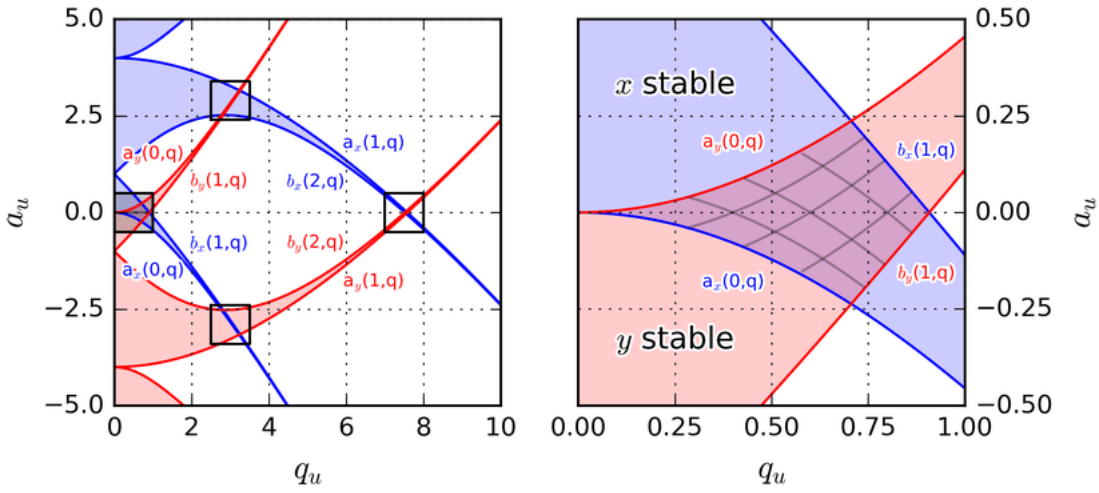

Figure 2.5: a-q-parameter space. Highlighted areas show the stability regions in a quadrupole beam guide. The right side provides an expanded view of the first region of stability, which is most commonly used because it is simply larger. Used with permission from J.M. Heinrich [9].

[1] When explained this way, the a-q-parameters appear to show up out of thin air. The parameters are actually obtained by solving the Mathieu equation. The authors would like to spare the reader from this derivation as it is well known and quite long.

2.2 Einzel lenses

An Einzel lens is an electrostatic component that can focus an incoming charged particle beam. Einzel meaning single referring to its unipotential construction. It can be seen as an analogue to an optical lens focusing incoming beams to a point. However, the working principles of the Einzel lens are very different to those of the optical lens.

2.2.1 The ideal Einzel lens

The ideal Einzel lens focuses an incoming beam of charged particles with velocity vectors parallel to the main axis of the lens to a point. The lens consists of three cylindrical electrodes separated by a short distance with a voltage applied to the middle one while the other two are typically grounded. This creates an electrical field between the electrodes which acts on an incoming particle in such way that the further away from the center of the lens the particle is, the stronger the electric field acting on it is, and the more the particle's trajectory is changed, as is illustrated in figure 2.6. The lens does not change the kinetic energy of a particle apart from when inside or close to it [10]. The focal length or refractive power of the lens depends on the potential of the middle electrode. A voltage comparable to that of the source yields a high refractive power [11].

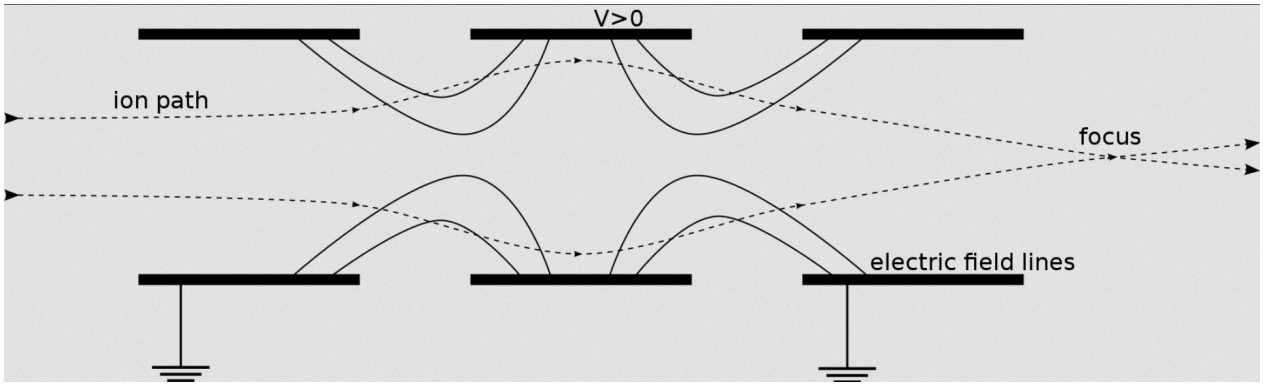

Figure 2.6: Two dimensional Einzel lens schematic, electric field lines generated by middle electrode. The trajectory of two anions flying from the left to the right are shown [12].

The change in radial velocity Δv_r of the charged particle passing between any pair of lens electrodes can be analytically calculated using the following equation,

$$\Delta v_\mathrm{r} = \int \frac{q|\boldsymbol{E}_\mathrm{r}(\boldsymbol{r}, x)|}{m\boldsymbol{v}_\mathrm{x}} \mathrm{d}\boldsymbol{x}, \tag{2.2}$$

with x-axis passing through the middle of the lens, and r is the direction normal to x. $|\boldsymbol{E}_\mathrm{r}(\boldsymbol{r}, x)|$ is the magnitude electrical field at a particular radial distance and distance across the electrode gap x and m is the mass of the particle [11].

2.2.2 Einzel lens in imperfect vacuum

One of the main limiting factors in this setup is gas leakage from the compressor section. The effects of which on the performance in Einzel lenses are well known and demonstrated here.

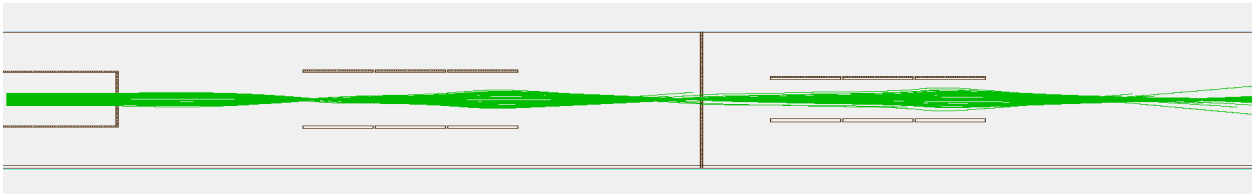

(a)

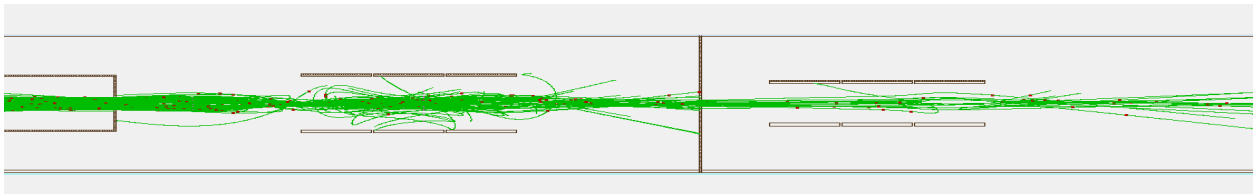

(b)

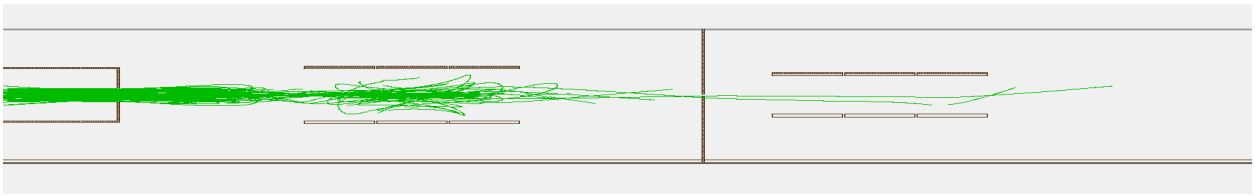

(c)

Figure 2.7: Parts a, b and c each show the trajectory of anions with a kinetic energy of 500 eV and mass 100 u from the source through the first and second Einzel lenses with differing gas pressures in the two chambers. Eventual collisions are marked in red. In part (a) the system is in vacuum. In part (b) both chambers are filled with helium at 0.1 Pa. In part (c) both chambers are filled with helium at 0.3 Pa.

Figure 2.7 above shows how the first and second Einzel lens in the setup behave with varying pressure within them. Note the significant loss of ions even with a relatively low pressure. The ions fired one at a time for all these examples, thus no ion-ion interaction is taken into account.

2.3 Deceleration

In this section the use of gas in the deceleration of ions is discussed.

2.3.1 Selection of buffer gas

Hugget and Menasian first demonstrated buffer gas damping of ion motion in a Paul trap by using a small amount of helium gas [13]. Nowadays, buffer gases are widely used in RF traps because when the ions are produced they can have a temperature above 10 K and thus have a large second-order Doppler shift. In the following section, the selection of buffer gas which is used in the deceleration anions in first quadrupole is discussed.

There are a number of parameters that need to be accounted for in the process of choosing a buffer-gas, the most significant ones are the stability of the gas, the atomic mass and gas particle's ability to conduct electricity. The latter can be investigated using the Paschen law.

2.3.2 Paschen's law

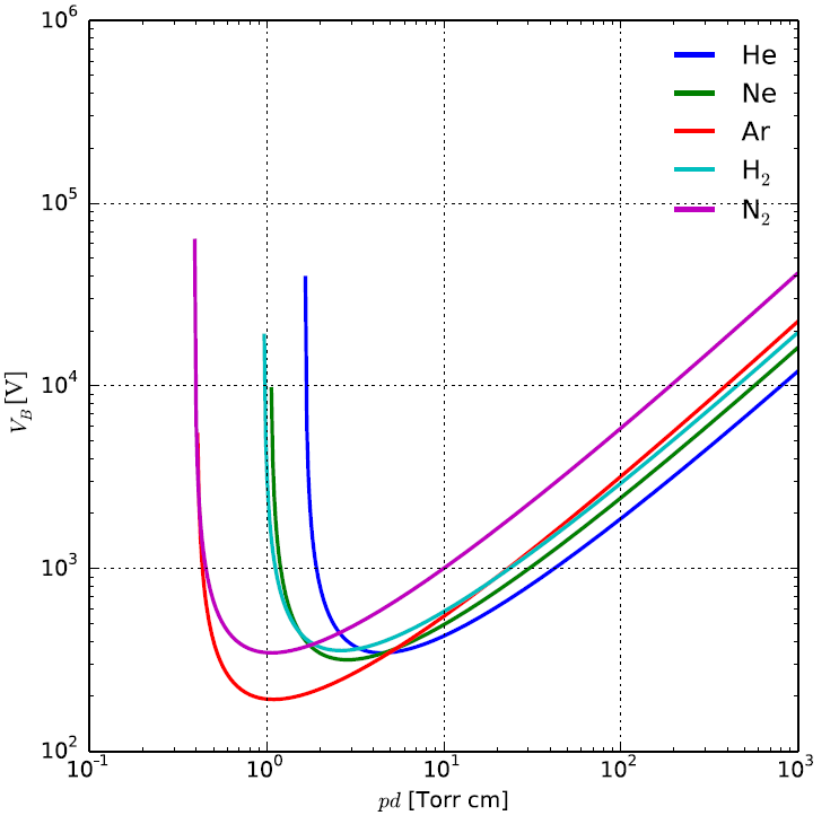

Figure 2.8: Paschen curves for helium, neon, argon, hydrogen and nitrogen. The breakdown voltage of gas (voltage required to start an discharge or electric arc through the gas) as a function of pd, the product between pressure and the gap length between electrodes, given in Torr cm [14].

Friedrich Paschen discovered an empirical relation between the voltage V_B needed to create an arc between two conductors at a given distance d and pressure p, which may be expressed

as,

$$V_{\mathrm{B}} = \frac{Bpd}{\ln(Apd) - \ln\ln(1+\gamma_{\mathrm{se}})}, \quad pd = \frac{e \cdot \ln(1+1/\gamma_{\mathrm{se}})}{A}, \tag{2.3}$$

where V_{B} is the breakdown (arc) voltage, p is the pressure in Pascal, A is saturation ionization in gas, B is the excitation and ionization energies in gas, d is the gap length and γ_{se} is the secondary electron emission coefficient. Secondary emission is a phenomenon where an initial particle of sufficient energy hitting a surface or passing through some material induces the emission of a secondary particle [15].

If a sufficient amount of gas leaks into a part of the setup with insulated electrodes, high voltages applied can ionize the gas, leading to an arc between two electrodes, short-circuiting them and therefore damaging the AC electronics driving them.

Another important property of the gas is its atomic mass, which should be low enough so that the vacuum pumps can handle difference of pressures between the different compartments but heavy enough to slow down the desired ions. The most common choice of gas in quadrupole ion traps is helium, not only because it is a noble gas and therefore non-reactive, but because it has a large enough mass to produce significant collisional cooling, while it is not large enough to cause significant scattering or dissociation during the collisions.

2.3.3 Collisional cross section - CCS

Due to the lack of a standard model for the collisional cross section of ions, that takes the ion charge into consideration, an estimation is required. In 2014 a study of the dynamics of biomolecular charge fragments was conducted by recording the time of flight (TOF) in a gas drift tube filled with helium, used in an trapped ion mobility spectrometer (TIMS). For sphere-like molecular ions an equation for the collisional cross section was presented [16],

$$\sigma = \frac{(18\pi)^{(1/2)}}{16} \frac{Q}{(k_{\mathrm{B}}T)(1/2)} \left[\frac{1}{m_I} + \frac{1}{m_{\mathrm{b}}}\right]^{1/2} \frac{1}{K} \frac{760}{P} \frac{T}{273.15} \frac{1}{N^*} \tag{2.4}$$

where K is the mobility value of a given ion in the buffer gas which was measured in the study, N^* is the number density of the target particles, Q is the charge of the ion, k_{B} is the Boltzmann constant, P is the pressure, T is the temperature and m_{I} and m_{b} refer to the masses of the molecular ion and buffer gas molecule, respectively.

An adaptation of equation (2.4) using the mobility values from the study [16] will be used in the simulations because it provides a better estimation for the ions collisional cross section.

Chapter 3

Method

To successfully achieve the goals of this project and understand its limitations, without exploring in detail each and every possible configuration, the setup should be simulated. Simulating the setup will allow for the characterization of the approximate behavior of the different components and their effect on the moving particles. In this way it can be determined whether the proposed setup has the ability to perform as expected, and if not, what changes to the setup may be required.

Simulations were performed in the SIMION 8.1 software using an exploratory approach. Different electrode voltages, ion masses and gas pressures were tested to give insights into the expected behavior of this setup in real life and also guide the decision-making process regarding what parts will be used in the deceleration stage and the capacity of the turbo pumps that will be required.

3.1 Simulating physics

By using simulation software, the complex problem of examining the trajectory of the ion beam and the physics behind each interaction can be approached, even if by the use of approximation. The insights gained can give an idea of what is to be expected from the setup and what potential problems might arise during experiments.

3.2 SIMION

SIMION is a simulation software package which aims at a broad audience and is used in industry as well as for academic purposes. It is primarily used to calculate particle trajectories influenced by magnetic and/or electric fields, but it can also handle aspects such as simpler particle collisions [17].

3.2.1 About SIMION

SIMION calculates electrostatic fields by solving boundary value problems and the Laplace equation, using a finite difference method. The voltages are approximated in points between the electrodes by summing the contributions from each electrode, using the Laplace equation's linear properties in the solution. The particle trajectory is then being calculated by using a Runge-Kutta method which works similar to the Euler method, calculating the new trajectory for each set time step [18].

Two important concepts regarding the accuracy of the particle trajectories are the potential array (PA) grid unit size and the trajectory quality factor (T.Qual). The PA grid unit size determines the size of the elements from which the electrode surfaces are constructed. This quantity can be seen as how many "pixels" make up the electrodes where more pixels obviously will make a curved surface appear less jagged. The scale is given in mm/grid unit, a lower value means that the electrodes have a higher resolution but also that the resolution of the resulting fields also increases. T.Qual decides the distance in grid units a particle travels before the trajectory is recalculated. A larger T.Qual value means that a shorter distance is traveled and therefore increases the simulation quality at the expense of performance. The opposite is true for a lower value. The default value of three corresponds to that of a particle moving one grid unit before the trajectory is recalculated. When it comes to simulation accuracy both the T.Qual and PA grid unit size work hand in hand. There is not much use highly refining the trajectory if the electromagnetic fields steering the ion are not also of high quality [18].

3.2.2 Potential array used

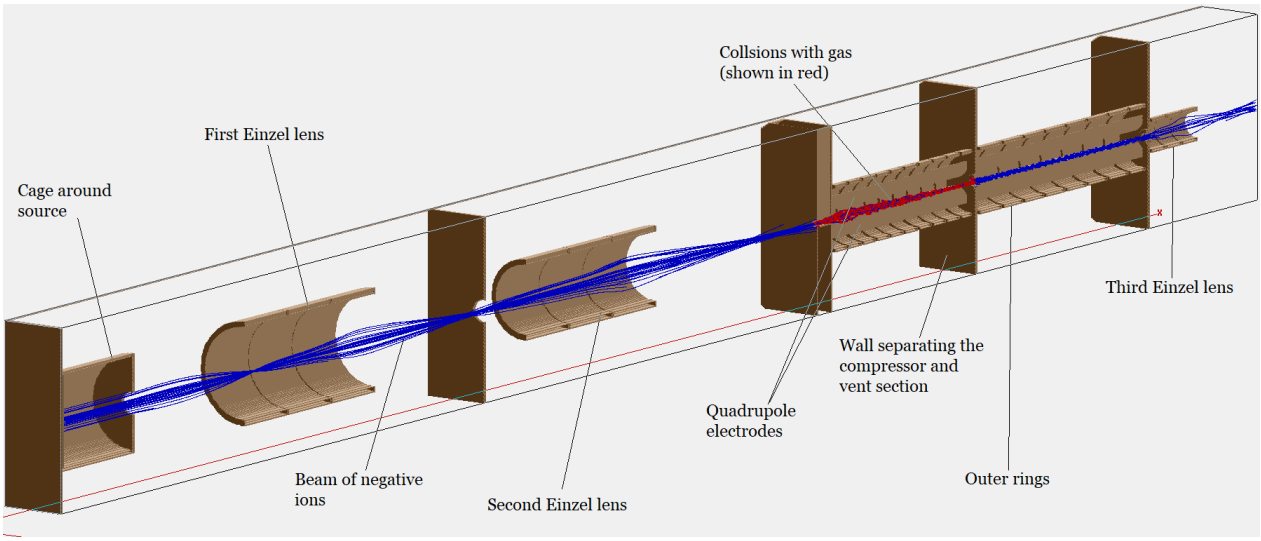

Figure 3.1: Half-section view in SIMION of the components in the first part of the beam line. Ions fly from the left to the right. The individual components are labelled.

The setup used in SIMION was implemented by Sylvain Maclot and Alexander Hinterberger. The beamline starts with the SNICS-II sputter source which produces ions in a energy range of $5 - 15\,\text{keV}$ [19]. A potential well is put around the source which is used as an initial ion deceleration down to a kinetic energy range of $50 - 500\,\text{eV}$. Because of the large voltage required in the initial deceleration, other components are protected from electrical discharges by putting a Faraday cage around the source as shown in figure 3.1. The first Einzel lens is used for focusing the anions into the next section where the second lens then focuses the beam into the compressor section. This is the section filled with helium gas used to further decelerate the beam down to $1\,\text{eV}$. The vent section serves to do away with most gas so that it is not to make it further down the beamline. The walls between each section serve to compartmentalize the gas used in the compressor section as much as possible. Even a small amount of gas can significantly disrupt the ion beam going through the Einzel lens, see figure 2.7. Additionally, as discussed in 2.3.2 if the gas is to make it close to the ion source, a large electrical discharge could occur, damaging the components. The quadrupole extending the entire length of the compressor and vent section is surrounded by a series of ring electrodes, such that a potential divider is created. A negative voltage is applied to the first ring in both the compressor and vent section creating a voltage gradient that "pulls" ions out towards the third Einzel lens.

Not shown in figure 3.1 are the turbo pumps used to remove gas leaking out of the compressor section. In SIMION this is not a problem since the pressure is set to zero everywhere with the exception of that specific section. In the beamline shown, there are turbo pumps in every section separated by a wall. The specifications of which are to be decided by the results of this report.

The setup used is quite large and therefore loading the potential arrays uses a relatively large amount of RAM. At least 8 gigabytes of RAM is required to be able to run any simulation without major problems. To accommodate for lower computer specifications the accuracy was lowered to a T.Qaul of three, which is reasonable and the PA grid unit size was set to $0.25\,\text{mm/gu}$, which was determined to have a good balance between performance and accuracy [18].

3.2.3 User program

SIMION allows users to run their own scripts through a user program, e.g. Lua. This feature can be utilized to simplify the control of the electrode voltages, compute results, export data, etc. During this project Lua was used to simulate an alternating time-dependent potential field in the quadrupole beam guide and to simulate the hard-sphere collisions in the compressor chamber. The latter was achieved by utilizing a slightly modified version of the standard hard-sphere collision model `hs1.lua` in SIMION. Furthermore, it was used to fine tune the electrode voltages of the Einzel lenses to an appropriate level, see appendix C.

3.3 Limitations

Simulations offer a time and cost-efficient means to examine the properties of the system but one must know the limitations of the approximations that are being made. This includes both the approximations made regarding the mathematical models used as well as the limitations of the software.

Since the beam consists of negatively charged particles they repel each other. This could have an influence on the trajectory and behavior of ions. The effect can be approximated in SIMION in two ways. Firstly, by setting the repulsion option to "beam repulsion" the particle trajectory is treated as a line of current in amps, used for time independent charges like in a steady stream of ions. The second by calculating the Coulomb interaction by treating each particle as a point charge, used for when the charge is time dependent. When calculating the charge repulsion the software makes the assumption that the electric fields created by the electrodes are not affected by the space charge of a particle. Any accurate calculation of the repulsion will also be much more computationally heavy due to the added complexity. In systems like the compressor where there is a large amount of ions in motion SIMION has no good way of dealing with repulsion. The amount of computation required is beyond the scope the software. For these reasons the space charge repulsion had to be neglected [18].

Differential pressure between different compartments could not be applied due to an unknown error in the user program implemented. The effect of which is that only one compartment can be pressurized at a time which in almost every scenario has to be the compressor section for obvious reasons. Whereas ideally there would be a greater than zero pressure in the vent section where additional collisions would be expected to occur.

When ion-gas collisions occur the software uses the hard-sphere model presented in Appendix B when calculating the transfer of energy. This model assumes a number of things, for example: elastic collisions, gas is unaffected as a whole, etc. This has the effect that all physical phenomena such as collisional ionization are neglected [18].

The drives creating the alternating potential in the quadrupoles is modeled as a sinusoidal form in SIMION whilst in the future setup a digital drive will be used. The difference between the two shown in figure 3.2. For the purpose of our simulations, the difference was deemed insignificant.

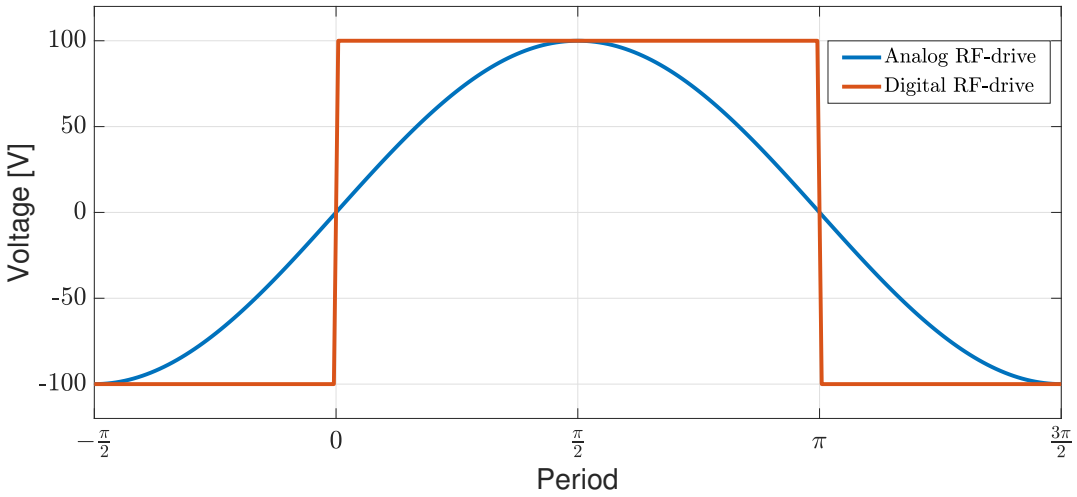

Figure 3.2: Difference between a digital and a sinusoidal (analog) RF-drive signal. The sinusoidal signal needs to ramp up before hitting its peak amplitude, the digital signal is either at maximum or minimum amplitude, there is no in between. Because of this, the digital spends more time at peak value, a lower RF-voltage can be used in a quadrupole driven by this type of signal. The operational frequencies of the drive will be in between 1 and 4 MHz.

There are also some physical limitations that have to be considered. The maximal amount of power the RF-drives can produce and not overheat in the proposed setup is limited to 100 W. The amount of power drawn can be calculated by the following equation,

$$P = 250 \left(\frac{\Omega}{10^6} \right) \left(\frac{V_{\text{rf}}}{500} \right)^2 \tag{3.1}$$

where P is the power in watts, Ω and V_{rf} are as defined in equation (2.1).

Chapter 4

Results and discussion

In this section the results will be presented and discussed. The results consist of the relevant values applied to the potential arrays and the pressures used in the simulations. The potentials need to guide a large portion of the ions through the chambers. The different pressures that were found to decelerate anions of varying energy and mass into the thermal range in the compressor.

4.1 Potential arrays - PAs

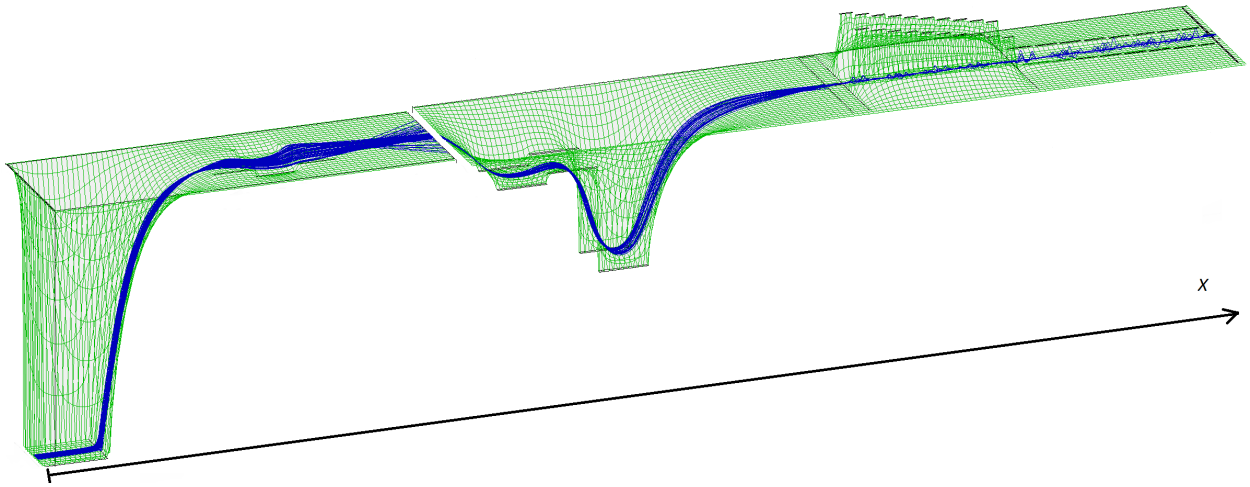

Figure 4.1: A potential surface induced by the DC electronics in the optimized setup. Regions with positive electrostatic potential are represented by a sunken map zone, while regions with a negative electrostatic potential are elevated. From this perspective, the negative ions, whose trajectories are displayed as blue lines, behave like balls accelerating down a hill and decelerating upwards as they travel from left to right. Note that the depth of surface is not to scale as the size was adjusted for visual clarity.

The electrode voltages applied to potential arrays in SIMION, whose values can be seen in Appendix A.2, were obtained through iterations using the Lua user program (see section

3.2.3) to maximize the transmission rate of the ion beam through the small apertures of the setup while decelerating the ions to kinetic energy range of $50 - 500\,\mathrm{eV}$ before they enter the compressor part of the setup.

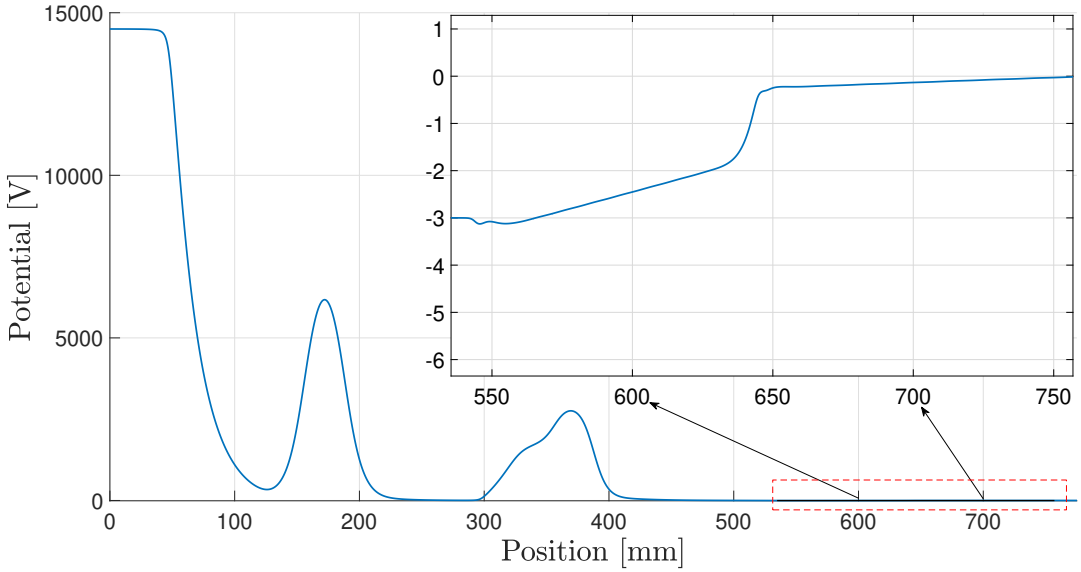

Figure 4.2: Potential perceived by a negative ion traveling from the source to the end of the vent section along the symmetry-axis. Shown in the top-right corner is an expanded view of the potential in the quadrupole. The potential in this section is the same in all potential array configurations used.

Figure 4.2 shows how the anions perceive the potential produced by the DC electronics along the x-axis of the quadrupole. The 500 eV kinetic energy setup is demonstrated; however, the difference between the 50 eV, 100 eV and 500 eV kinetic energy is only seen near the source. The negatively charged particles are accelerated by a positive potential and decelerated by a negative potential slope. The gradient, shown in the expanded view in figure 4.2 is created by the ring electrodes surrounding the length of the quadrupole. It was discovered early on that even a small potential well has the effect of trapping ions due to their low kinetic energy at this stage. To resolve this issue a gradual increase of the potential inside the quadrupole beam guide had to be implemented.

4.2 Distribution of energy

In this section an overview of the overall change in energy of anions moving through all components of the setup is presented. Results provide evidence that the setup works as intended. No distinction between the thermal and kinetic energy of the anions is made.

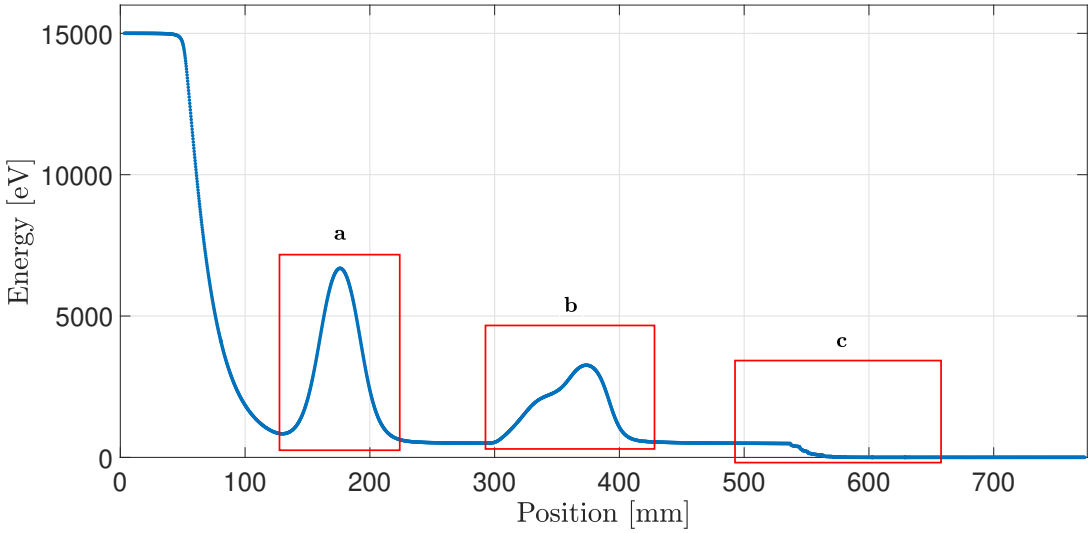

Figure 4.3: Deceleration as the ions fly through the setup. Demonstrated with the kinetic energy of one negative ion as a function of distance traveled using the 500 eV PA setup. The bumps (a) and (b) is are caused by the first and second Einzel lenses. (c) shows the final deceleration in the compressor. The energy curve follows the potential curve seen in the previous figure 4.2, showing the direct relation of the electrostatic potential on the anions.

The initial deceleration occurs by using a steep potential slope between 0-125 mm as seen in figure 4.3. In parts (a) and (b) the acceleration followed by the consecutive deceleration of the anion when passing through both the first and the second Einzel lens can be observed. This is because if any ion passes between any two pairs of electrodes in an Einzel lens, the change of velocity described by equation (2.2), which evaluated and summed over both electrode pairs is equal to zero. The change in velocity is asymmetrical in the second Einzel lens because of the asymmetrical potential applied to the electrodes of the lens to re-focus the diverging beam. Part c shows the final deceleration through collisions with gas in the compressor chamber which only makes up only a small amount of the total change in kinetic energy. The largest change in energy occur due to a change in potential, which is the reason for the similarities with figure 4.2.

4.3 Deceleration in the compressor and vent sections

In this section the results for the deceleration in the compressor and vent compartments are presented. At the very end of the vent section the distribution of kinetic energy is to be centered at, and not broader than 1 eV.

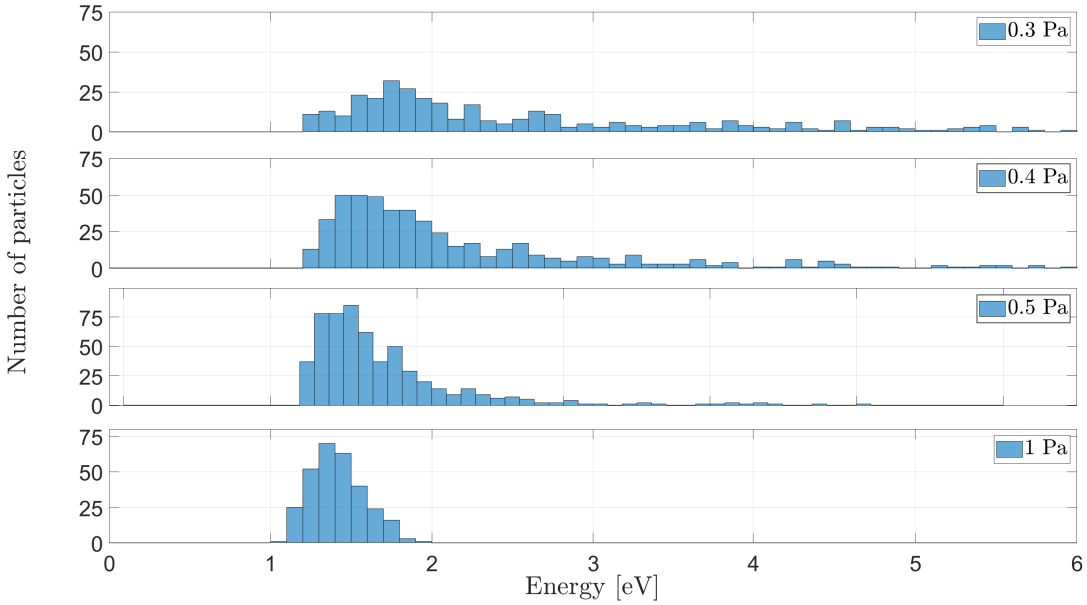

Figure 4.4: Change in energy spread due to change in pressure, using a mass of 12 u and an energy of 50 eV when entering the compressor.

The distribution of kinetic energy for mass 12 u and various pressures measured at 775 mm can be seen in figure 4.4, the very end of the vent section. The distribution is tighter and shifts closer to 1 eV with higher pressure. The width and center of the distribution increases with a lower pressure. This is due to the fact that there is a lower probability of ion-gas collisions in lower pressure.

Table 4.1: Pressure required in the compressor section in order to decelerate the anions and achieve the desired distribution of kinetic energy.

Mass [u]	Pressure [Pa] for 50[eV]	Pressure [Pa] for 100[eV]	Pressure [Pa] for 500[eV]
12	2	2.85	3
50	4	4.85	5
100	6	5	7
400	7	7	7.8
720	8	8	10.5

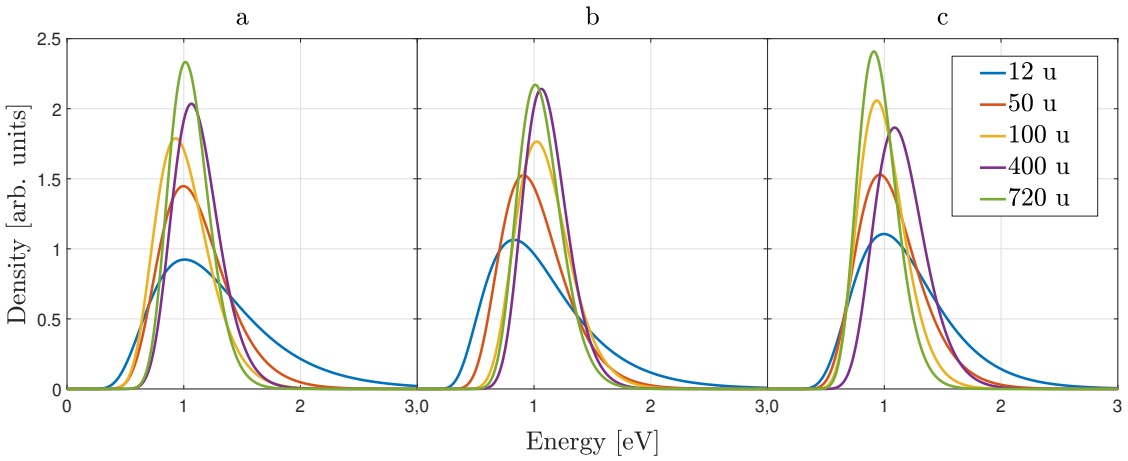

Figure 4.5: Distribution of kinetic energy in the negative ion beam at the very end of the vent section, with energies a) 50 eV, b) 100 eV, and c) 500 eV before entering the compressor section. Inverse Gaussian fits were made with the data obtained through simulations, where the distribution were centred as close to 1 eV as possible. Ion masses 12, 50, 100, 400 and 720 u were used. The broadest full width at half-maximum for all three figures is 0.98 eV and 0.17 eV is the largest distance of any peak to 1 eV.

The results presented in figure 4.5, show that by the using pressures presented in table 4.1, the energy could be reduced to a distribution centered at 1 eV with full-width half maximum of less than 1 eV, as measured the end of the vent section, for masses in the range to be used and relevant entrance energies.

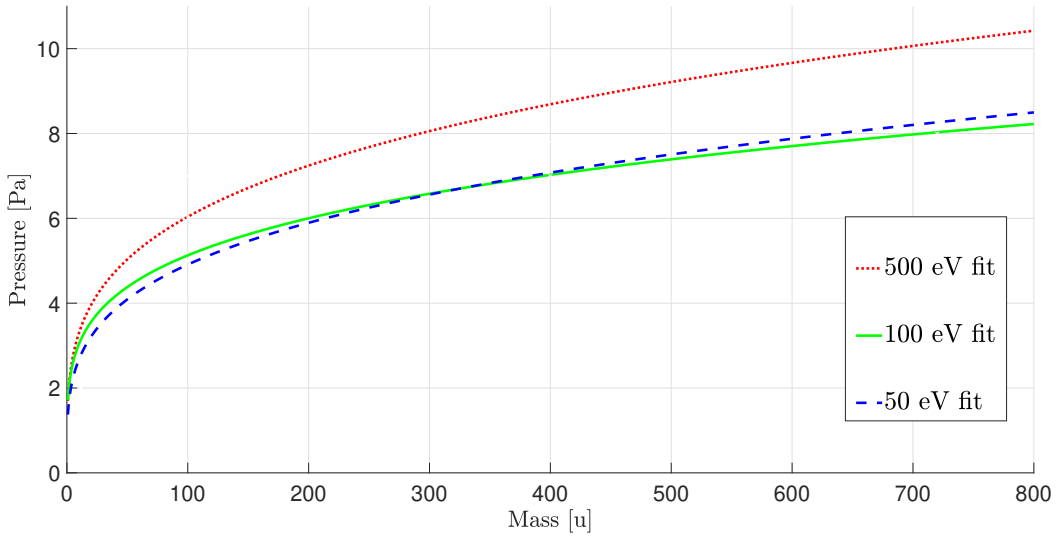

Figure 4.6: Relationship between mass and pressure for a kinetic energy distribution centered around 1 eV. The FWHM of the distribution is kept within the 1 eV threshold. Ions with kinetic energies 50, 100, and 500 eV when entering the compressor are shown. The curves were made to fit the data points presented in table 4.1, using an power equation of the type $a \cdot x^b$.

In figure 4.6 the three different fits show the required pressure for the three cases of initial energy 50, 100 and 500 eV. The most prominent aspect is that the 50 eV and the 100 eV fits are almost identical. This can be explained by the fact that the difference in kinetic energy between them is small. In addition to the potential slope being gradual for both cases, meaning that the potential of the ring electrodes could be optimized even more by using a steeper slope in order the extract the anions faster for the lower kinetic energy.

4.4 Transmission

The transmission rate for the three cases of the kinetic energy are seen figure 4.7. Three major drops are seen, these are the result of the anions hitting the walls between the different compartments. The shape of the transmission curve between 540 mm-775 mm is dependent on the pressure used in the compressor chamber, as higher pressures result in lower transmission rates at this section. The lowest rate of transmission is at 8 % when using the lower kinetic energy setup of 50 eV, a consequence of the increased refractive power of the Einzel lens for higher ion beam energies. The reason for studying cases with a lower energy setup despite having a lower transmission rate is due to the fact that using a higher deceleration potential at 50 mm results in a smaller energy distribution going in to the compressor chamber. In turn this leads to a higher level of control over anions in the quadrupole, besides the lower pressure needed to reduce the energy of the ions.

In the physical setup, gas is expected to be present in the compartments housing the Einzel lenses. Determining the amount of gas in these sections is however beyond the scope of SIMION and the effects are well known, see figure 2.7. Therefor it can be concluded that

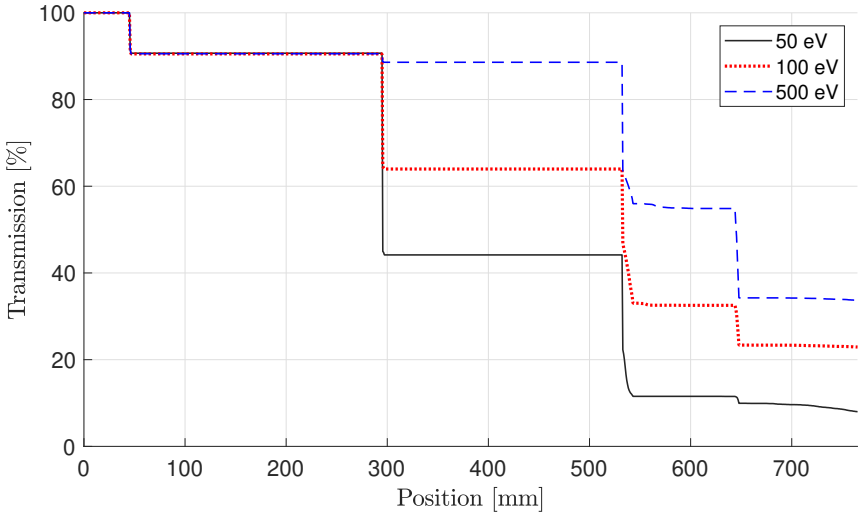

Figure 4.7: Einzel lenses transmission in percent, for the 50, 100 and 500 eV kinetic energy setups. All the sudden drops correspond to anions hitting the walls dividing the different compartments. The transmissions rate at the entrance of the compressor chamber 540 mm for the 50, 100, and 500 eV kinetic energies are 11%, 32%, and 59%, respectively. Note the correlation between the higher kinetic energy and the transmission rate of the anion beam. This is a consequence of the increased refractive power of the Einzel lens for higher ion beam energies.

the transmission percentages seen here are significantly higher than they would be in reality.

4.5 Areas of improvement

The accuracy and precision of the results can be improved by simulating a larger number of anions, as well as increasing the grid unit size and the T.Qual in SIMION to improve the precision of the trajectory calculations.

The ions produced from the SNICS-II were considered to have a single discreet energy rather than the Gaussian distribution that the source would generate, the FWHM of which is unknown.

Another aspect that was not taken into consideration due to time and software restrictions was the beam repulsion. This can be solved by using the built-in charge repulsion function in SIMION but it has the downside of having computational complexity on the order of $O[N^2]$ in addition to being time independent. The latter can be partially bypassed by updating the amplitude of the repulsion when a significant percentage of the beam is lost e.g. after the small apertures between the compartments. Another approach would be to solve the Poisson's equations outside SIMION which would result in a more accurate repulsion values and lower computation complexity based on the method used but it is more difficult to implement [18].

During the simulations the beam was considered to be parallel to the symmetry axis of the beam guide coming out from the source, which is not the case because of the source's nature. Taking the angle of the generated beam into account would result in a decreased transmission rate that was considered to be equal to zero in this project.

Chapter 5

Conclusion

The SIMION software package could be utilized in obtaining the optimized values for all adjustable electrodes in the setup, resulting in a compressor trap that could successfully decelerate anions entering with kinetic energies 500 eV, 100 eV and 50 eV into the kinetic energy range of 1 eV using helium gas.

For masses in a range between 12 and 720 u, a maximal pressure of 10.5 Pa was required. Using these values a transmission of at least 8% could be achieved. These results have led to valuable insight in what kind of pressure difference is to be expected in the different compartments. This was important in guiding the group in making the decision of what specification turbo pump will be used. Furthermore, these results led to the re-design of this part of the beam guide, whereas previous designs did not have electrostatic ring electrodes around the quadrupole beam guide. The added electrodes helped push the anions through the beam guide preventing them from getting stuck in chamber section.

Bibliography

[1] Angelus. *Quadrupole mass analyzer [pnline]. 2011 [Cited 2021 May 5]. Available from.* URL: https://commons.wikimedia.org/wiki/File:Quadrupole_mass_analyzer.svg. (CC BY-SA 3.0) http://creativecommons.org/licenses/by-sa/3.0/.

[2] Einstein A. *Einstein's Proposal of the Photon Concept- a Translation of the Annalen der Physik Paper of 1905; 1965. [Cited 2021 Maj 6]. Available from.* URL: http://astro1.panet.utoledo.edu/~ljc/PE_eng.pdf.

[3] Andersson S. Bruhn F. Hedman J. Karlsson L. Lunell S. Nilson K. et al. *Atom- och molekylfysik.* First edition. Lund. Repro Fysikum, 2005. ISBN: 9163115956.

[4] Feifel R. L'Huillier A. Lindroth E. Zhaunerchyk V. Gisselbrecht M. Dahlström M. *Project Plan. Attosecond chronoscopy of electron wave-packets probing entanglement and time-ordering of quantum processes.*

[5] National Electrostatics Corp. Source of Negative Ions by Cesium Sputtering - SNICS II [internet]. Wisconsin USA [cited: 8 Maj 2021]. URL: http://www.pelletron.com/wp-content/uploads/2017/02/SNICS-v2.pdf.

[6] Major F.G. Gheorghe V.N. Werth G. *Charged Particle Traps.* atomic, optical, and plasma physics. Springer-Verlag, 2005. ISBN: 3-540-22043-7.

[7] Wolfgang P, Steinwedel H, et al, inventors; Wolfgang P, assignee. Apparatus for separating charged particles of different specific charges. United States Patent and Trademark Office 2939952. Issued DEC 24 1953.

[8] Kriesch A. *Paul-Trap [internet]. 2006 [Cited 2021 Maj 5]. Available from.* URL: https://commons.wikimedia.org/wiki/File:Paul-Trap.svg. (CC BY-SA 3.0) http://creativecommons.org/licenses/by-sa/3.0/.

[9] Heinrich JM. *A Be+ Ion Trap for H2+ Spectroscopy. Atomic Physics [physics.atom-ph]. Sorbonne Université, Faculté des Sciences et Ingénierie, 2018. English. tel-01889833. Available from.* URL: https://tel.archives-ouvertes.fr/tel-01889833/file/JMHeinrich_thesis.pdf.

[10] Hinterberger F. Ion optics with electrostatic lenses [internet]. Geneva: Conseil Européen pour la Recherche Nucléaire (CERN); 2006. [Cited 2021 Maj 5]. Available from. URL: http://cds.cern.ch/record/1005034/files/p27.pdf;.

[11] Helmut Liebl. *Applied Charged Particle Optics.* Germany: Springer-Verlag, 2008. ISBN: 978-354071924.

[12] Schnieri. *Einzel lens schematic drawing [internet]. 2017 [Cited 2021 Maj 8]. Available from.* URL: https://commons.wikimedia.org/wiki/File:Einzel_lens_schematic_drawing.svg. (CC BY-SA 4.0), url=https://creativecommons.org/licenses/by-sa/4.0/deed.en.

[13] A. Kellerbauer et al. "Buffer gas cooling of ion beams". In: *Nuclear Instruments and Methods in Physics Research Section A: Accelerators, Spectrometers, Detectors and Associated Equipment* 469.2 (2001), pp. 276–285. ISSN: 0168-9002. DOI: https://doi.org/10.1016/S0168-9002(01)00286-8. URL: https://www.sciencedirect.com/science/article/pii/S0168900201002868.

[14] Krishnavedala. *File:Paschen curves.svg — Wikimedia Commons, the free media repository [Online].* 2014 [cited 2021 May 8]. 2020. URL: https://commons.wikimedia.org/w/index.php?title=File:Paschen_curves.svg&oldid=518729213. (CC BY-SA 4.0), url=https://creativecommons.org/licenses/by-sa/4.0/deed.en.

[15] Friedrich Paschen. "Ueber die zum Funkenübergang in Luft, Wasserstoff und Kohlensäure bei verschiedenen Drucken erforderliche Potentialdifferenz". In: *Annalen der Physik* 273.5 (1889), pp. 69–96. DOI: https://doi.org/10.1002/andp.18892730505. URL: https://onlinelibrary.wiley.com/doi/abs/10.1002/andp.18892730505.

[16] Diana Rosa Hernandez et al. "Ion dynamics in a trapped ion mobility spectrometer". In: *Analyst* 139 (8 2014), pp. 1913–1921. DOI: 10.1039/C3AN02174B. URL: http://dx.doi.org/10.1039/C3AN02174B.

[17] Scientific Instrument Services (SIS). SIMION Ion and Electon Optics Simulator 2019 [internet]. Available from. URL: https://simion.com/.

[18] Scientific Instrument Services (SIS). SIMION 2019 supplimental documentation [internet]. Available from. URL: https://simion.com/info/index.html.

[19] Roy Middleton. A Negative Ion Cookbok[Online]. Department of Physics. University of Pennsylvania. Philadelphia. October 1989 (Revised 1990). [cited: 8 Maj 2021]. URL: https://www.pelletron.com/cookbook.pdf.

[20] Daniele L. Marchisio and Rodney O. Fox. "Hard-sphere collision models". In: *Computational Models for Polydisperse Particulate and Multiphase Systems*. Cambridge Series in Chemical Engineering. Cambridge University Press, 2013, pp. 214–265. DOI: 10.1017/CBO9781139016599.007.

[21] Carlo Cercignani. "The Boltzmann Equation". In: *The Boltzmann Equation and Its Applications*. New York, NY: Springer New York, 1988, pp. 40–103. ISBN: 978-1-4612-1039-9. DOI: 10.1007/978-1-4612-1039-9_2. URL: https://doi.org/10.1007/978-1-4612-1039-9_2.

Appendix A

Simulation parameters

In this chapter the optimized electrode values and the rest of the simulation parameters are presented.

A.1 PA's

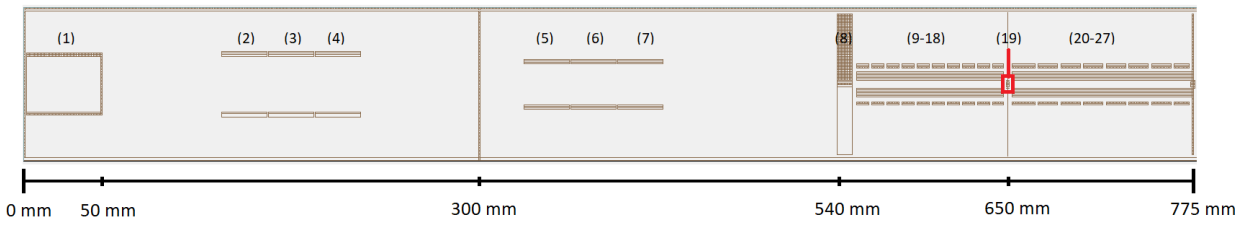

Figure A.1: A slice view along the x-axis of the simulated setup in SIMION that shows electrodes and their corresponding number.

Table A.1: Voltage values of the electrodes for the 50 eV setup. The table contains electrode number which can be seen in figure A.1 and the voltage of each electrode.

Electrode	Voltage [V]	Electrode	Voltage [V]	Electrode	Voltage[V]
1	14 950	10	−570	19	−0.305
2	0	11	−540	20	−40
3	400	12	−510	21	−35
4	0	13	−480	22	−30
5	500	14	−450	23	−25
6	400	15	−420	24	−20
7	1430	16	−390	25	−15
8	−1	17	−360	26	−10
9	600	18	−330	27	−5

Table A.2: Voltage values of the electrodes for the 100 eV setup. The table contains electrode number which can be seen in figure A.1 and the voltage of each electrode.

Electrode	Voltage [V]	Electrode	Voltage [V]	Electrode	Voltage[V]
1	14 900	10	−570	19	−0.305
2	0	11	−540	20	−40
3	1000	12	−510	21	−35
4	0	13	−480	22	−30
5	1000	14	−450	23	−25
6	1500	15	−420	24	−20
7	3150	16	−390	25	−15
8	−2	17	−360	26	−10
9	−600	18	−330	27	−5

Table A.3: Voltage values of the electrodes for the 500 eV setup. The table contains electrode number which can be seen in figure A.1 and the voltage of each electrode.

Electrode	Voltage [V]	Electrode	Voltage [V]	Electrode	Voltage[V]
1	14 500	10	−570	19	−0.305
2	0	11	−540	20	−40
3	8000	12	−510	21	−35
4	0	13	−480	22	−30
5	1700	14	−450	23	−25
6	3000	15	−420	24	−20
7	50	16	−390	25	−15
8	−3	17	−360	26	−10
9	−600	18	−330	27	−5

A.2 Other parameters

Table A.4: Values of the collisional cross section (CCS) and the angular frequency of the quadrupole Ω that were used in the simulations.

Mass [u]	CCS [m^2]	Ω [Hz]
12	9.5×10^{-19}	4.33×10^6
50	1.03×10^{-18}	2.12×10^6
100	1.12×10^{-18}	1.50×10^6
400	1.66×10^{-18}	7.50×10^6
720	2.16×10^{-18}	5.59×10^5

Appendix B

Hard-Sphere collision Models

Hard-sphere collision is a model of particle interactions based on collisions between smooth, spherical particles with identical (monodisperse) or different (polydisperse) densities ρ and diameters d. This model is used for its simplicity: particle mass m and diameter are conserved, and other processes are excluded. Assuming that the particles are smooth spheres means that the particle's angular momentum L is also conserved, and hence only the velocity of the particle must be accounted for in the kinetic equations. In other words, the particle's velocities can be written as an explicit function of the velocities prior to the collision, coefficient of restitution and the the particles masses[20].

The starting equation for the model is the following Boltzmann kinetic equation,

$$\delta_t f + \boldsymbol{u} \cdot \delta_{\mathrm{x}} f + \delta_{\mathbf{u}} \cdot (\boldsymbol{A} f) = \mathbb{C}, \tag{B.1}$$

In the equation above $f(t, \boldsymbol{x}, m, \hat{u})$ is the velocity number density function, t is time, $\boldsymbol{x}$ is spatial vector, m is the mass of the particle, $\boldsymbol{u}$ is the particle velocity, $\boldsymbol{A}$ is an acceleration, which can depend on fluid drag and gravity for the gas-particles depending on the variant of the used model. $\mathbb{C}$ represents the particle collisions.

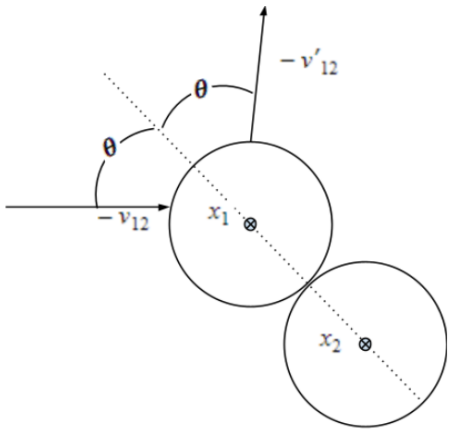

Figure B.1: A schematic drawing of a direct collision between two hard spheres, where $\boldsymbol{v}_{12}$ and $\boldsymbol{v}'_{12}$ are the velocity difference before and after the collision respectively, θ is the collision angle whose value is such that $\cos\theta$ is positive when collisions occur.

In the case of monodisperse hard-sphere collisions, the change in the number-density function $\mathbb{C}$ due to elastic collisions obeys the following integral form [21],

$$\mathbb{C} = \frac{6}{\pi d}\int_{\mathbb{R}^3}\int_{\mathbb{S}^+}[f^{(2)}(\boldsymbol{x},\boldsymbol{v}'_1;\boldsymbol{x}-\mathrm{d}\boldsymbol{x}_{12}\,,\boldsymbol{v}'_2)-f^{(2)}(\boldsymbol{x},\boldsymbol{v}_1;\boldsymbol{x}-\mathrm{d}\boldsymbol{x}_{12}\,,\boldsymbol{v}_2)]|\boldsymbol{v}_{12}\cdot\boldsymbol{x}_{12}|\,\mathrm{d}\boldsymbol{x}_{12}\,\mathrm{d}\boldsymbol{v}_2\,, \quad \text{(B.2)}$$

where d is the particle diameter, $f^{(2)}$ is a pair correlation function,

$$\boldsymbol{x}_{12} = -\frac{\boldsymbol{x}_1-\boldsymbol{x}_2}{|\boldsymbol{x}_1-\boldsymbol{x}_2|}, \quad \text{and } \boldsymbol{v}_{12}=\boldsymbol{v}_1-\boldsymbol{v}_2,$$

with x_{12} being the collision vector (in the direction between the particles centers), and $\boldsymbol{v}_{12}$ being the velocity difference before a collision (see figure B.1). Post collision quantities are denoted by a prime symbol. $\mathbb{S}^+$ is a surface which consists of the unit half sphere where $\boldsymbol{v}_{12}\cdot\boldsymbol{x}_{12} = -\boldsymbol{v}'_{12}\cdot\boldsymbol{x}_{12} = |\boldsymbol{v}_{12}|\cos\theta > 0$. θ is the collision angle. Due to the fact the collisions model used in the simulations considers collsions to be elastic, only the elastic collision model will be examined.

Equation (B.2) has a unique equilibrium solution defined by $\mathbb{C}=0$. This Maxwell-Boltzman distribution is calculated as follows:

$$f_{\mathrm{eq}}(\boldsymbol{v}) = \frac{\alpha_{\mathrm{p}}}{(2\pi\Theta)^{3/2}}\exp\left\{-\frac{|\boldsymbol{v}-\boldsymbol{U}_{\mathrm{p}}|^2}{2\Theta_{\mathrm{p}}^2}\right\},$$
$$\boldsymbol{U}_{\mathbf{p}} = \frac{1}{\alpha_{\mathrm{p}}}\int \boldsymbol{v} f\,\mathrm{d}\boldsymbol{v}\,, \quad \Theta_{\mathrm{p}} = \frac{1}{3\alpha_{\mathrm{p}}}\int|\boldsymbol{v}-\boldsymbol{U}_{\mathrm{p}}|^2 f\,\mathrm{d}\boldsymbol{v}$$

where $\boldsymbol{U}_{\mathrm{p}}$ is the mean velocity and Θ_{p} is the particle energy.

Appendix C

Lua-code

```
-- SIMION Lua workbench program for deceleration part of the ion project ATTOHALLEN
--
-- Created by S. Maclot
-- modified by T. Alhaskir 2021/03


simion.workbench_program()
-------------------------------------
-- Creating files
-------------------------------------

stamp = os.date("_%Y-%m-%d-%H%M%S")
local fh
local ir = assert(io.open('s.txt', "w"))

----------------------------
-- Local variables for ion counters
----------------------------

-- Position 1
local xcross1 = 0               -- ion position along x where the counter is located
local xlast1 = {}               -- use to calculate the counter
local count1 = 0                -- Counter

-- Position 2
local xcross2 = 250             -- ion position along x where the counter is located
local xlast2 = {}               -- use to calculate the counter
local count2 = 0                -- Counter

-- Position 3
local xcross3 = 450             -- ion position along x where the counter is located
local xlast3 = {}               -- use to calculate the counter
local count3 = 0                -- Counter

-- Position 4
local xcross4 = 475             -- ion position along x where the counter is located
local xlast4 = {}               -- use to calculate the counter
local count4 = 0                -- Counter


----------------------------
-- Collision model
----------------------------

-- import standard HS1 collision model from this directory.
simion.import("collision_hs1_deceleration.lua")

adjustable _gas_area_start_x_mm = 0                                     -- Start of the gas area along x (mm)
adjustable _gas_area_stop_x_mm = 520                            -- Stop of the gas area along x (mm)
--adjustable _gas_area_compressor_start_x_mm = 230      -- Start of the gas area for the compressor along x (mm)
--adjustable _gas_area_compressor_stop_x_mm = 410               -- Stop of the gas area for the compressor along x (mm)

-- adjustable _pressure_pa      = 1.0                                      -- Variable for calculation reason and to override
      collision_hs1.lua
-- adjustable _residual_pressure_pa_ = 0.001                    -- Pressure in the previous and next section of the
     compressor (Pa) -- 0.001 Pa = 10-5 mbar
-- adjustable _compressor_pressure_pa   = 1.0                   --  Pressure in the compressor (Pa)

-----------------------------------------------
-- Quadrupole
-----------------------------------------------


-- Variables adjustable during flight:

```

```
64  local pe_update_each_usec      = 0.05   -- potential energy display
65                                          -- update period (microsec)
66                                          -- (for display purposes only)
67
68  -- Variables adjustable only at beginning of flight:
69
70  local effective_radius_mm              = 2.0   -- half the minimum distance between
71                                                                  -- opposite rods (mm)
72  local phase_angle_deg                  = 0.0   -- entry phase angle of ion (deg)
73  adjustable _frequency_hz           = 1.5E6 -- RF frequency (Hz)
74  adjustable _rfvolts                        = 200   -- RF voltage for quadrupole
75
76  adjustable _max_TOF_in_quad_usec       = 200   -- Maximum time for ion TOF before killing (usec)
77  adjustable _splatPosition_mm           = 540 -- The position where the particle is killed
78
79  -------------------- DC Voltage
80  local dcvolts = 0       -- variable
81
82
83  -- internal variables
84  local last_pe_update = 0.0 -- last potential energy surface update time (usec)
85
86  local start_position_RF_ON_x_mm = 237   -- Position along X where the RF field start to be calculated
87  local stop_position_RF_ON_x_mm = 475    -- Position along X where the RF field start to be calculated
88
89  -- SIMION segment called by SIMION to set adjustable electrode voltages
90  -- in the current potential array instance.
91  -- NOTE: this is called frequently, multiple times per time-step (by
92  -- Runge-Kutta), so performance concerns here can be important.
93  function segment.fast_adjust()
94          if ion_px_mm >= start_position_RF_ON_x_mm and ion_px_mm < stop_position_RF_ON_x_mm then         -- To save time:
                start to put voltage on quadrupole rods only when entering the quadrupole region
95                local omega = _frequency_hz * (1E-6 * 2 * math.pi)
96                local theta = phase_angle_deg * (math.pi / 180)
97
98                local tempvolts =
99                sin(ion_time_of_flight * omega + theta) * _rfvolts + dcvolts
100
101               adj_elect11 =   tempvolts
102               adj_elect12 = - tempvolts
103
104         end
105 end
106 ------------------------------------------------
107 -- Function to get the ion kinetic energy
108 ------------------------------------------------
109
110 local function get_ke()
111   local speed = math.sqrt(ion_vx_mm^2 + ion_vy_mm^2 + ion_vz_mm^2)
112   return speed_to_ke(speed, ion_mass)
113 end
114
115
116
117
118 ------------------------------------------------
119 -- Main function of the code
120 ------------------------------------------------
121
122
123 -- This trick first runs the other_actions segment defined previously
124 -- by the HS1 collision model and then runs our own code.
125 local previous_other_actions = segment.other_actions  -- copy previously defined segment.
126
127 -- SIMION segment called by SIMION after every time-step.
128 --local is_initialized
129 function segment.other_actions()
130
131         -- Ion counter --
132                 if ((xlast1[ion_number] or ion_px_mm) < xcross1) == (ion_px_mm >= xcross1) then
133                         count1 = count1 + 1
134                 --      print(count1)
135                 --      print(ion_number,get_ke())
136                         fh:write(ion_number, "␣", xcross1, "␣", ion_py_mm,"␣", ion_pz_mm, "␣", get_ke(), "\n")
137                 end
138                 if ((xlast2[ion_number] or ion_px_mm) < xcross2) == (ion_px_mm >= xcross2) then
139                         count2 = count2 + 1
140                         fh:write(ion_number, "␣", xcross2, "␣", ion_py_mm,"␣", ion_pz_mm, "␣", get_ke(), "\n")
141                 end
142                 if ((xlast3[ion_number] or ion_px_mm) < xcross3) == (ion_px_mm >= xcross3) then
143                         count3 = count3 + 1
144                         fh:write(ion_number, "␣", xcross3, "␣", ion_py_mm,"␣", ion_pz_mm, "␣", get_ke(), "\n")
145                 end
146                                 if ((xlast4[ion_number] or ion_px_mm) < xcross4) == (ion_px_mm >= xcross4) then
147                         count4 = count4 + 1
148                         fh:write(ion_number, "␣", xcross4, "␣", ion_py_mm,"␣", ion_pz_mm, "␣", get_ke(), "\n")
149                 end
150
151         xlast1[ion_number] = ion_px_mm
152         xlast2[ion_number] = ion_px_mm
153         xlast3[ion_number] = ion_px_mm
154         xlast4[ion_number] = ion_px_mm
155
156                 -- Run the collision model in the selected area
157         if ion_px_mm >= _gas_area_start_x_mm and ion_px_mm <= _gas_area_stop_x_mm then
```

```
158                 previous_other_actions()
159         end
160
161
162                 -- Now run the RF code
163
164                 --if  ion_px_mm > start_position_RF_ON then -- To save computational time, the RF only start with the ion
                        approach the quadrupole region.
165                 --      if not is_initialized then
166                                 -- Convert to SI units.
167                 --              local q = ion_charge * 1.602176462*10^-19 -- (C/e)
168                 --              local m = ion_mass * 1.66053886*10^-27    -- (kg/u)
169                 --              local omega = _frequency_hz * 2 * math.pi -- (rad/cycle)
170                 --              local r0 = effective_radius_mm / 1000 -- (m/mm)
171
172                                 -- Compute octupole stability constants [Hagg 1986]
173                 --              local a4 = 32 * q * _dcvolts / (m * omega^2 * r0^2)
174                 --              local q4 = 16 * q * _rfvolts / (m * omega^2 * r0^2)
175
176                                 -- Print stability constants.
177                                 --print(string.format("m/z=%g,a4=%g,q4=%g", ion_mass/ion_charge, a4, q4))
178                 --              is_initialized = true -- only execute once
179                 --end
180
181                 -- Update potential energy surface display periodically.
182                 -- The performance overhead of this in non-PE views is only a few percent.
183                 -- NOTE: the value inside abs(...) can be negative when a new ion is flown.
184                 if abs(ion_time_of_flight - last_pe_update) >= pe_update_each_usec then
185                         last_pe_update = ion_time_of_flight
186                         sim_update_pe_surface = 1    -- Request a PE surface display update.
187                 end
188
189            -- Kill the ion if stay too long in the quadrupole or after a ceratin point to make the simulations shorter
190                 if ion_time_of_flight > _max_TOF_in_quad_usec or ion_px_mm > _splatPosition_mm  then
191                         ion_splat = -1
192                 end
193
194         --end
195
196 end
197
198 -- SIMION segment called by SIMION to override time-step size on each time-step.
199 function segment.tstep_adjust()
200    -- Keep time step size <= X usec.
201    ion_time_step = min(ion_time_step, 0.01)  -- X usec
202 end
203
204
205
206
207 ------------------------------------------------
208 -- Rerun variables
209 ------------------------------------------------
210 -- adjustable _potenial = 0
211  adjustable _startPotenialA
212  adjustable _endPotenialA
213  adjustable _steg
214  --adjustable _startPotenialB
215 -- adjustable _endPotenialB
216  --adjustable _startPotenialC
217  --adjustable _endPotenialC
218  adjustable _electrode_numA
219 -- adjustable _electrode_numB
220  --adjustable _electrode_numC
221 -- adjustable _derivative
222  local nions = 0
223  local trans ={}
224  local pA ={}
225  local iterationsA = (_endPotenialA-_startPotenialA)/_steg -- number of iterations
226 --local iterationsB = (_endPotenialB-_startPotenialB)/_steg
227 --local iterationsC = (_endPotenialC-_startPotenialC)/_steg
228 local A_voltage
229 local B_voltage
230 local C_voltage
231
232 function segment.initialize() ---- calculates the number of initialized particles
233   nions = ion_number
234 end
235
236 ------------------------------------------------
237 -- Rerun code
238 ------------------------------------------------
239 adjustable i_0
240
241 function segment.flym()
242         sim_rerun_flym = 1
243   for i=1,iterationsA do
244         --for j = 1,iterationsB do
245         --      for k = 1,iterationsC do
246       --Prepare for this run.
247       A_voltage = _startPotenialA+_steg*i
248      -- B_voltage = _startPotenialB+_steg*j
249          -- C_voltage = _startPotenialC+_steg*k
250                 run()
251    end
```

```
252 end
253
254
255 function segment.fast_adjust()
256         --local electrode = _electrode_num
257         --local volt = _startPotenial+_steg*ion_run
258         if          _electrode_numA == 0 then
259
260         elseif _electrode_numA < 10 then
261                 adj_elect[_electrode_numA] = A_voltage
262                 --adj_elect[_electrode_numB] =  B_voltage
263                 --adj_elect[_electrode_numC] =  C_voltage
264         --elseif _electrode_numA == 13 then
265                 --for i=1,10 do
266                 --      adj_elect[i+12] =  _startPotenial+_steg*ion_run + i * _derivative
267                 --end
268         --elseif _electrode_numA == 24 then
269         --      for i=1,8 do
270                 --      adj_elect[i+12] =  _startPotenial+_steg*ion_run + i * _derivative
271         --      end
272         end
273 end
274 ------------------------------------------------
275 -- At the beginning of every run
276 ------------------------------------------------
277
278 function segment.initialize_run()
279   fh = assert(io.open('output'..tostring(ion_run)..stamp..'.txt', "w")) -- creates a new txt file for each run and gives
          it a time stamp
280   print("New␣run,␣number",ion_run,"\n")
281  --segment.fast_adjust()
282 end
283 ------------------------------------------------
284 -- At the end of every run
285 ------------------------------------------------
286
287 function segment.terminate_run()
288         print('transmission:', count2 / nions * 100,"%","\n","Run␣number"..tostring(ion_run),"\n")
289         --fh:write('transmission at x=0:', count1 / nions * 100,"%","\n","Potenial over electrod"..tostring(_electrode_num
              ).. "is = ",_startPotenial+ion_run*_steg,"\n")
290         --fh:close()
291         --ir:write('transmission at x=0:', count1 / nions * 100,"%","\n","Potenial over electrod"..tostring(_electrode_num
              )..." is = ",_startPotenial+ion_run*_steg,"\n")
292
293         print(count1) -- print the number of ions in counter 1
294         print(count2)   -- print the number of ions in counter 2
295         print(count3)   -- print the number of ions in counter 3
296         print(count4)   -- print the number of ions in counter 4
297
298         ir:write("run","␣",ion_run,"␣",count2 / nions * 100,"%","␣",A_voltage)  --[[",B_voltage," ",C_voltage," ","\n")]]
              --
299         trans[ion_run] =count2
300         -- reseting the counters after each run
301      count1=0
302          xlast1 = {}
303          count2=0
304          xlast2 = {}
305          count3=0
306          xlast3 = {}
307          count4=0
308          xlast4 = {}
309         if ion_run == iterations then
310
311         --sorting function
312         local function indexsort(trans)
313                 local idx = {}
314                 for i = 1, #trans do idx[i] = i end -- build a table of indexes
315                 -- sort the indexes, but use the values as the sorting criteria
316                 table.sort(idx, function(a, b) return trans[a] > trans[b] end)
317                 -- return the sorted indexes
318                 return (table.unpack or unpack)(idx)
319         end
320         print(indexsort(trans))
321
322         end
323
324 end
```